Clays and Clay Minerals, Vol. 54, No. 2, 195–208, 2006.

COMPARISONS OF STRUCTURAL Fe REDUCTION IN SMECTITES BY BACTERIA AND DITHIONITE: AN INFRARED SPECTROSCOPIC STUDY

KANGWON LEE[1], JOEL E. KOSTKA[2] AND JOSEPH W. STUCKI[1,*]

[1] Department of Natural Resources and Environmental Sciences, University of Illinois at Urbana-Champaign, Urbana, Illinois, USA

[2] Department of Oceanography, Florida State University, Talahassee, Florida, USA

Abstract—The reduction of structural Fe in smectite is mediated either abiotically, by reaction with dithionite, or biotically, by Fe-reducing bacteria. The effects of abiotic reduction on clay-surface chemistry are much better known than the effects of biotic reduction. Since bacteria are probably the principal agent for mediating redox processes in natural soils and sediments, further study is needed to ascertain the differences between biotic and abiotic reduction processes. The purpose of the present study was to compare the effects of dithionite (abiotic) and bacteria (biotic) reduction of structural Fe in smectites on the clay structure as observed by infrared spectroscopy. Three reference smectites, namely, Garfield nontronite, ferruginous smectite (SWa-1), and Upton, Wyoming, montmorillonite, were reduced to similar levels by either *Shewanella oneidensis* or by pH-buffered sodium dithionite. Each sample was then analyzed by Fourier transform infrared spectroscopy (FTIR). Parallel samples were reoxidized by bubbling O_2 gas through the reduced suspension at room temperature prior to FTIR analysis. Redox states were quantified by chemical analysis, using 1,10-phenanthroline. The reduction level achieved by dithionite was controlled to approximate that of the bacterial reduction treatment so that valid comparisons could be made between the two treatments. Bacterial reduction was achieved by incubating the Na-saturated smectites with *S. oneidensis* strain MR-1 in a minimal medium including 20 mM lactate. After redox treatment, the clay was washed four times with deoxygenated 5 mM NaCl. The sample was then prepared either as a self-supporting film for OH-stretching and deformation bands or as a deposit on ZnSe windows for Si−O stretching bands and placed inside a controlled atmosphere cell also fitted with ZnSe windows. The spectra from bacteria-treated samples were compared with dithionite-treated samples having a similar Fe(II) content. The changes observed in all three spectral regions (OH stretching, M_2−O−H deformation, and Si−O stretching) for bacteria-reduced smectite were similar to results obtained at a comparable level of reduction by dithionite. In general, the shift of the structural OH vibration and the Si−O vibration, and the loss of intensity of OH groups, indicate that the bonding and/or symmetry properties in the octahedral and tetrahedral sheets changes as Fe(III) reduces to Fe(II). Upon reoxidation, peak positions and intensities of the reduced smectites were largely restored to the unaltered condition with some minor exceptions. These observations are interpreted to mean that bacterial reduction of Fe modifies the crystal structures of Fe-bearing smectites, but the overall effects are modest and of about the same extent as dithionite at similar levels of reduction. No extensive changes in clay structure were observed under conditions present in our model system.

Key Words—Cycles, Ferruginous Smectite, Garfield, Montmorillonite, Nontronite, Oxidation, Redox, Reduction, *Shewanella*, Upton.

INTRODUCTION

The oxidation state of Fe in the crystal structures of smectite clay minerals plays an important role in determining the surface and colloidal chemistry and the physical behavior of the clay. The omnipresence of microorganisms in the soil and recent discoveries that bacteria can reduce structural Fe(III) to Fe(II) in smectite clay minerals (Stucki and Getty, 1986; Stucki *et al.*, 1987; Kostka *et al.*, 1996; Wu *et al.*, 1988) also lead to the expectation that bacterial activity in soils and sediments is a determining factor in the alteration of soil properties and behavior. This expectation was confirmed by Favre and co-workers (Favre *et al.*, 2002, 2004; Boivin *et al.*, 2002) who found changes in cation exchange capacity (CEC) that could be attributed, at least in part, to natural changes in smectite Fe oxidation state due to bacterial activity.

Kostka *et al.* (1999) reported that smectite dissolution occurs during bacterial reduction if organic acids and chelating agents are present in the reducing medium. Kim *et al.* (2003, 2004) and Dong *et al.* (2003) took that idea one step further and, based on transmission electron microscopy (TEM), X-ray diffraction (XRD), and energy-dispersive X-ray analysis (EDX), proposed that bacterial reduction causes major changes in the smectite structure, including dissolution and reprecipitation as illite and other Fe-bearing minerals. Lacking in these studies, however, was an assessment of the extent to which smectite dissolution occurs during bacterial reduction in the

* E-mail address of corresponding author:
jstucki@uiuc.edu
DOI: 10.1346/CCMN.2006.0540205

absence of chelating agents and the ultimate potential for bacterial processes to invoke massive irreversible changes in smectite structure. Consequently, a more complete understanding is needed of the effects of bacterial reduction on smectite structure.

Previous studies of dithionite-reduced smectites found significant changes in the clay structure as a result of Fe redox processes (Stucki and Roth, 1976; Manceau *et al.*, 2000b; Fialips *et al.*, 2002a, 2000b; Huo, 1997; Huo *et al.*, 2004). Yan *et al.* (1996a, 1996b, 1996c, 1996d) and Yan and Stucki (1999, 2000) demonstrated a direct relation between structural Si−O vibrations and the vibrational energy of adsorbed interlayer H_2O molecules, confirming a direct link between the clay crystal structure and the chemical behavior in the interlayer. Stucki and Roth (1977) and Gates *et al.* (1996) found, respectively, that changes in structural Fe oxidation state also alters the structural Si−O vibrational and nuclear energies. In these studies the extent of structural changes and the reversibility of such changes clearly depended on the level of reduction that was achieved by the dithionite treatment. Such an assessment has not been performed with bacteria-reduced smectites, but could have significant bearing on our understanding of the potential for structural changes in smectite due to natural redox cycles. The objective of the current study was to fill this gap by reporting structural changes, as measured by infrared (IR) absorption spectroscopy, in various Fe-bearing smectites reduced to modest levels either by bacteria or by dithionite.

MATERIALS AND METHODS

Clay preparation

The clays used in this study were Garfield nontronite sample API 33a (Garfield, Washington, obtained from Ward's Natural Science Establishment), ferruginous smectite sample SWa-1 (Grant County, Washington, obtained from the Source Clays Repository of The Clay Minerals Society), and Upton montmorillonite (Upton, Wyoming, obtained from American Colloid Company). The clay samples were dispersed by stirring overnight in high-purity H_2O then homoionically saturated with Na^+ by washing with 1 M NaCl solution. The <0.05 μm particle-size fraction was collected and excess salts removed by repeated washing by centrifugation using 5 mM NaCl solution, then freeze dried. Further purification was achieved using the method described by Manceau *et al.* (2000a). The structural formulae for the respective samples are (Manceau *et al.*, 2000a)

Garfield:
$Na_{0.81}(Si_{7.22}Al_{0.78})(Fe^{3+}_{3.64}Fe^{2+}_{0.01}Al_{0.32}Mg_{0.04})O_{20}(OH)_4$;
SWa-1:
$Na_{0.87}(Si_{7.38}Al_{0.62})(Fe^{3+}_{2.67}Fe^{2+}_{0.01}Al_{1.08}Mg_{0.23})O_{20}(OH)_4$;
Upton:
$Na_{0.72}(Si_{7.82}Al_{0.18})\ (Al_{3.06}Fe^{3+}_{0.30}Fe^{2+}_{0.02}Mg_{0.65})O_{20}(OH)_4$.

Structural Fe reduction and reoxidation

The clay minerals were reduced for 1 week using a pure culture of *Shewanella oneidensis* strain MR-1 which was isolated from the anoxic sediments of Lake Oneida, New York, and has been the subject of many physiological and genetic studies concerning bacteria−Fe(III) mineral interactions (Nealson and Saffarini, 1994). *S. oneidensis* is a facultative anaerobe and an obligate-respiratory bacterium, incapable of fermentative growth (Scott and Nealson, 1994).

Standard methods for the culture of anaerobic bacteria were used, but modified for clay reduction experiments as described by Kostka *et al.* (1996). The minimal culture medium was prepared according to Kostka and Nealson (1998), the pH adjusted to 7, and dispensed into serum bottles. Carbon substrate (lactate) was added from sterile, anoxic stocks to 20 mM final concentration. Smectite clay was added to a particle concentration of 1 g L^{-1}. Culture bottles were sealed with butyl rubber stoppers and incubated at 30ºC in the dark. All manipulations of culture samples were carried out under strictly anoxic conditions within a Coy anaerobic chamber (90% N_2, 10% H_2). Inoculum cultures were grown aerobically to late log phase on the same minimal medium, and cells were added to clay-reduction experiments to a final cell density of 10^8 cells mL^{-1} (determined by epifluorescence microscopy, Kostka *et al.*, 2002). Heat-killed controls were prepared by heating with microwave radiation until boiling (Kostka *et al.*, 1996).

Other samples of the same smectites were also reduced chemically with sodium dithionite. A 30 mg portion of the freeze-dried clay was dispersed by stirring in 20 mL of deionized water overnight. After addition of 10 mL of buffer solution (2 parts of 1.2 M sodium citrate ($Na_3C_6H_5O_7{\cdot}2H_2O$) and 1 part of 1 M sodium bicarbonate ($NaHCO_3$)) and establishment of a continuous N_2 purge, the suspension was heated in a water bath to 70ºC and 150 mg of dithionite salt was added. The reaction was allowed to proceed for 10 min for Garfield and SWa-1 and for 10, 120 or 240 min for Upton. The samples were then centrifuge washed four times with deoxygenated 5 mM NaCl solution.

A second set of both bacteria- and dithionite-reduced samples was reoxidized after washing with 5 mM NaCl by bubbling O_2 gas through the reduced suspension for 24 h at room temperature. The actual levels of Fe reduction and reoxidation (*i.e.* Fe(II) contents) were obtained by chemical analysis using the 1,10-phenanthroline (phen) method (Komadel and Stucki, 1988).

IR spectroscopy

Infrared spectra were measured at a beam incident angle of 90º using a Midac M2000 FTIR spectrometer and spectral analyses were performed using the GRAMS/32 program, following the procedures of Fialips *et al.* (2002a, 2000b) with the following changes.

Absorbance spectra were obtained from 50 scans with a nominal resolution of 4 cm^{-1} in the 4000−680 cm^{-1} region. The structural OH-stretching region, 3800−3000 cm^{-1}, and M_2−O−H deformation region, 950−680 cm^{-1}, were collected using self-supporting films in a controlled-atmosphere cell (Angell and Schaffer, 1965), fitted with ZnSe windows (Janos Technologies, Inc., Keene, New Hampshire), to prevent reoxidation and hydration. The self-supporting films were prepared inside an inert-atmosphere glove box using 2.5 to 3 mg of sample per cm^2 collected by vacuum filtration onto a 15 mm × 0.025 μm pore size Millipore membrane filter. The films with filter membranes were dried over P_2O_5 in a desiccator inside the glove box overnight then placed under vacuum for 12−24 h. The dried film was removed from the membrane filter, placed in a cardboard film holder with a 15 mm diameter opening, and inserted into the controlled-atmosphere cell inside the glove box (Fialips *et al.*, 2002b; Angell and Schaffer, 1965). The cell with sample was then removed from the glove box and placed in the FTIR sample compartment through a specially constructed access port. The intensity of each spectrum was normalized to the sample mass of the film. Oxidized and reoxidized samples were treated identically to the reduced sample, except sample handling occurred outside the glove box with no special precautions to preclude atmospheric oxygen.

Spectra in the Si−O stretching region were acquired using deposits of ~0.5 mg/cm^2 of smectite onto a 25 mm diameter ZnSe window. Since the exact amount of sample in the beam was uncontrolled under these conditions, the spectra were normalized only to an arbitrarily chosen intensity value to allow an easy comparison of relative peak positions. Otherwise, samples were treated and analyzed exactly the same as the self-supporting films.

Fourier transform infrared spectra of the pure bacterial cultures were also obtained (Kostka *et al.*, 1996). The pure culture of *S. oneidensis* strain MR-1 in the minimal M1 medium (Myers and Nealson, 1988), containing the same composition used to inoculate the clay suspensions, was washed four times with 5 mM NaCl solution. A 1.5 mL portion of the washed suspension, containing ~10^8 cells/mL, was then deposited onto a 25 mm diameter ZnSe window and analyzed in the same manner as the samples. The spectra (Figure 1) revealed four characteristic peaks in the 2800−3300 cm^{-1} region and eight in the 1100−1700 cm^{-1} region. Assignments for these bands according to Maquelin *et al.* (2002) and Benning *et al.* (2004) (Table 1) include modes from H_2O, lipids, amides, nucleic acids, polysaccharides and carboxylic acid in the cell structure and sheath (Choo-Smith *et al.*, 2001; Kirschner *et al.*, 2001).

Except for IR bands due to polysaccharides, which overlap Si−O modes in the 900−1200 cm^{-1} region, and water bands in the 3200−3400 cm^{-1} region, which raise the low-frequency background of the OH-stretching peaks, the bacterial spectrum is largely non-overlapping with the regions of interest in the smectite spectra (Figure 1). Little change in the spectrum of the bacteria was observed after reaction with the smectites.

RESULTS AND DISCUSSION

The IR spectrum of smectites is greatly influenced by the type and distribution of octahedral cations (Robert and Kodama, 1988; Madejová *et al.*, 1994; Gates, 2005). The vibrational energy of structural OH shifts according to the metal cations to which it is coordinated, as

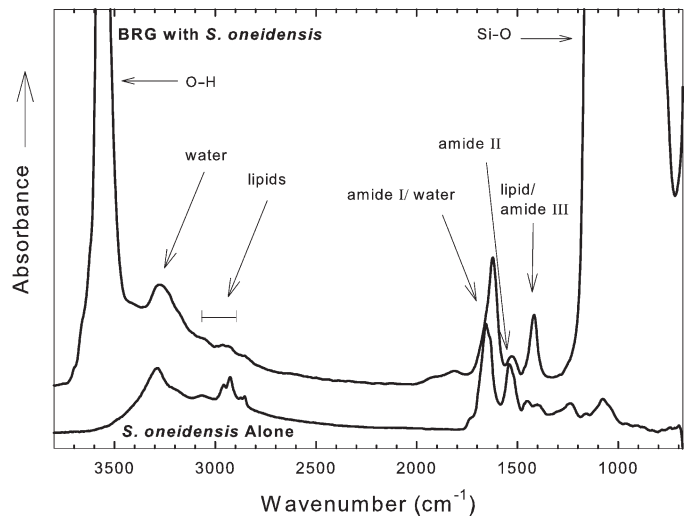

Figure 1. Representative FTIR absorbance spectra of *S. oneidensis* MR-1 whole cells. Assignments of main bands with numbers in parentheses are indicated in Table 1. A spectrum of bacteria-reduced Garfield nontronite (BRG) is also shown to illustrate the extent of overlap of peak positions with *S. oneidensis*.

Table 1. Frequencies and band assignments for the FTIR spectrum of the *S. oneidensis* MR-1 whole cells (modified from Maquelin *et al.*, 2002, and Benning *et al.*, 2004).

Band	Wavenumber (cm^{-1})	Assignment	Main group	Note
1	~3292	ν O−H and ν N−H	Water	Water/amide A
2	~2958	ν_{as} C−H of $-CH_3$	Lipids	Methyl group in fatty acids
3	~2926	ν_{as} C−H of $>CH_2$	Lipids	Methylene group in fatty acids
4	~2877	ν_{sy} C−H of $-CH_3$	Lipids	Methyl group in fatty acids
4	~2853	ν_{sy} C−H of $>CH_2$	Lipids	Methylene group in fatty acids
5	~1732	ν >C=0 of esters	Membrane lipids	Fatty acids
6	~1650	ν >C=0	Amide I	Protein (amide I of α- or β-helical structures)
7	~1542	δ N−H and ν C−N	Amide II	Protein
8	~1453	δ_{as} C−H of $>CH_2$/ δ_{as} C−H of $-CH_3$	Lipid Amide III	Broad methylene peaks with varying positions; protein
9	~1389	ν_{sy} C=O of COO^-	Carboxylic acids	Stretching carboxylates
10	~1240	ν_{as} P=O of $>PO_2^-$	Nucleic acid	Stretching phosphodiester backbone of the nucleic acids (DNA and RNA)
11	~1164	ν C−0	Polysaccharides	Ring vibrations of polysaccharides
12	~1079	ν_{as} P=O of PO_2^-	Nucleic acid	Stretching phosphodiester backbone of the nucleic acids (DNA and RNA)

ν = stretching; δ = deformation; as = asymmetric; sy = symmetric.

illustrated in the deconvolution of the OH-stretching bands for Garfield nontronite (Figure 2, Table 2), ferruginous smectite SWa-1 (Figure 3, Table 3), and Upton montmorillonite (Figure 4, Table 4). The component bands for Upton are attributed to [AlAl]OH, [AlMg]OH, [MgFe]OH and [AlFe]OH (Figure 4, Table 4). A small residual band due to adsorbed H_2O, and/or a trioctahedral $[M]_3OH$ feature, is also often included on the high-frequency (~3670 cm^{-1}) side of the peak. Upton contains much less structural Fe (2.40% by weight, 0.429 mmol/g) than either Garfield (24.15% by weight, 4.325 mmol/g) or SWa-1 (18.33% by weight, 3.282 mmol/g) and the Fe is believed to be dispersed in the structure, so few if any [FeFe]OH clusters are expected (Vantelon *et al.*, 2001; Gates, 2005). Clusters of [FeFe]OH are present, however, in Garfield and SWa-1, centered at ~3570 cm^{-1} (Figures 2 and 3).

Garfield nontronite

OH-stretching vibration bands. The OH-stretching band of unaltered Garfield nontronite (UG) is centered at 3570 cm^{-1} and contains a shoulder at ~3530 cm^{-1} (Figure 2). The assignment of the principal component of this band is clearly to the dioctahedral $[Fe(III)]_2OH$ environment for the OH group (Goodman *et al.*, 1976; Russell *et al.*, 1979; Fialips *et al.*, 2002b)), but the assignment of the 3530 cm^{-1} band is uncertain. Fialips *et al.* (2002a) discussed several different structural configurations that could explain a peak at this position, including $[Fe(II)]_2OH$, *cis*-occupied octahedra, tetrahedral Al substitution, and a splitting due to symmetric and asymmetric OH vibrations. In each of these cases, however, the relatively high intensity of this component band (~1/3 of the total) is difficult to reconcile with other structural information (*e.g.* the unaltered Garfield has no Fe(II) and the number of sites associated with the other configurations is expected to be relatively small). This feature is absent from the spectra of other Fe-rich smectites. If one of the latter attributions is to be made, a proportionately larger absorptivity would be required for that absorber compared to the principal $[Fe(III)]_2OH$.

Upon reduction of structural Fe(III) to Fe(II), the overall position of the OH-stretching band shifted from 3570 cm^{-1} to 3560 cm^{-1} if reduced by bacteria (BRG) or to 3542 cm^{-1} if reduced by dithionite for 10 min (RG10) (Figure 5a). The reduction levels were 0.735 and 0.995 mmole Fe(II)/g in BRG and RG10, respectively (Table 5). The shifts in band position are consistent with previous observations (Fialips *et al.*, 2002b) and reflect the change in OH vibrational energy due to conversion of the octahedral cation occupancy from an entirely $[Fe(III)]_2OH$ environment to combinations of $[Fe(III)]_2OH$, [Fe(III)Fe(II)]OH, and possibly $[Fe(II)]_2OH$. The greater shift in RG10 is probably due to the greater Fe(II) content compared to BRG. The intensity of the peaks also decreased, reflecting a possible loss of OH groups from the clay structure. These shifts in peak position and intensity are significant in terms of the change in energy, but are rather small compared to the complete disappearance of a distinct structural OH-stretching band that occurs if the non-

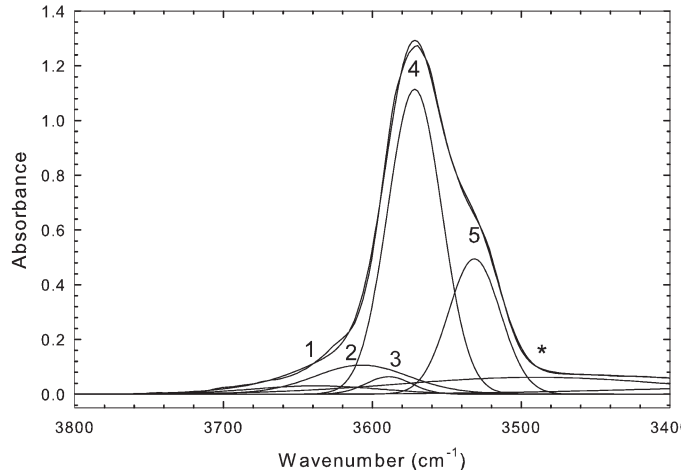

Figure 2. IR spectrum of the OH-stretching region in unaltered Garfield nontronite (UG) deconvoluted to reveal the peak positions for the possible M_2OH environments. Band assignments and areas are reported in Table 2.

tronite is fully reduced (>90%) by dithionite (Fialips *et al.*, 2002b), indicating that reduction by either bacteria or minimal dithionite treatment created relatively minor changes in the clay structure.

The observed changes in peak position and intensity were largely reversed when the smectite was reoxidized (Figure 5b). The dithionite-reduced-reoxidized Garfield (ROG10) recovered its original position and shape, including the shoulder at 3530 cm^{-1}, indicating that the reduction process failed to invoke the extensive changes in clay structure that occur upon complete reduction (Fialips *et al.*, 2002a, 2000b). The OH-stretching peak from the bacteria-reduced-reoxidized sample (BROG) was restored to the original unaltered position, also indicating that no catastrophic structural changes had occurred during reduction; but, interestingly, the shoulder at 3530 cm^{-1} was absent after reoxidation. While this difference is subtle, it provides evidence that the structural changes occurring during bacteria-mediated redox reactions may differ slightly from those mediated by dithionite. With further study, this difference could prove to be important in elucidating the assignment of the 3530 cm^{-1} band as well as specific structural changes due to bacterial reduction.

OH-bending vibration bands. The principal feature in the M_2−O−H deformation region of Garfield nontronite (Figure 5c) is a strong band at 822 cm^{-1} assigned to $[Fe(III)]_2$−O−H, with shoulders at 843 and 790 cm^{-1}. Stucki and Roth (1976) assigned the 843 cm^{-1} shoulder to $[Fe(III)]_2$−[OH], but assignment of the band at 790 cm^{-1} is less certain. Typically it is assigned to Si−O associated with amorphous silica or finely divided quartz, or to Fe−Mg−OH (Russell *et al.*, 1979; Stucki and Roth, 1976; Goodman *et al.*, 1976; Fialips *et al.*, 2002b); but the Mg content is too low to justify the latter and the fact that it was lost after either reduction treatment indicates that it must be related to Fe, not Si-O. A similar phenomenon was observed by Fialips *et al.* (2002a, 2000b).

Reduction of structural Fe by either bacteria or dithionite shifted the main peak at 822 cm^{-1} to lower frequency and decreased its intensity (Figure 5c). The 843 cm^{-1} peak decreased in intensity with bacterial reduction (BRG), and after dithionite reduction (RG10) it was either lost completely or replaced by a peak at 870 cm^{-1}. The differences between dithionite- and bacteria-treated samples could easily be attributed to the small difference in the levels of reduction.

Table 2. Positions (cm^{-1}) and relative spectral areas (A) of the OH-stretching bands of the unaltered (UG), bacteria-reduced (BRG), and 10 min dithionite-reduced (RG10) Garfield nontronite.

Band	Assignment	UG		BRG		RG10	
		(cm^{-1})	A (%)	(cm^{-1})	A (%)	(cm^{-1})	A (%)
1	AlAlOH	3638	3.8	3627	2.4	3626	1.3
2	FeAlOH	3607	10.3				
3	FeMgOH	3589	2.8				
4	FeFeOH	3572	58.3	3570	62.1	3551	74.6
5	FeFeOH	3532	24.8	3536	35.5	3530	20.8
Total			100.0		100.0		96.7*

* Residual is in an undetermined band for H_2O.

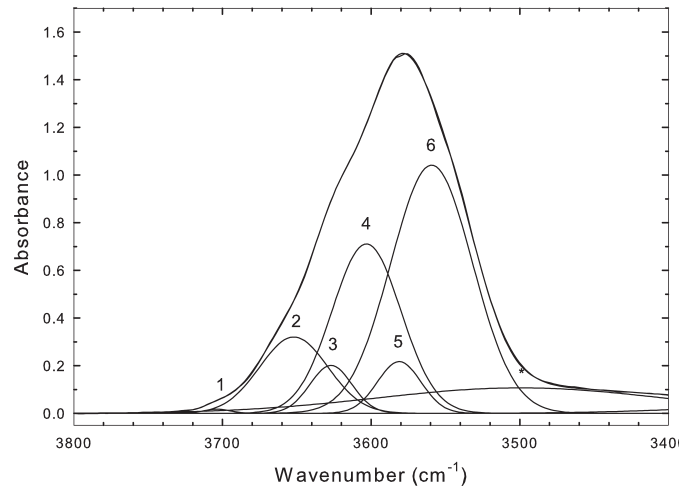

Figure 3. IR spectrum of the OH-stretching region in unaltered ferruginous smectite (US) deconvoluted to reveal the peak positions for the possible M_2OH environments. Band assignments and areas are reported in Table 3.

Reoxidation of both samples BRG and RG10 restored the peaks to their original unaltered positions and features (samples BORG and ROG10, respectively), except a small difference was noted in the effect of reduction-reoxidation on the 843 cm^{-1} band (Figure 5c). The effect of bacterial reduction is, therefore, generally consistent with the dithionite treatment for the levels of reduction achieved, follows the same trend as in the OH-stretching region, and invokes only minor changes in structure.

Si–O-stretching vibration band. The position of the Si–O-stretching band (Figure 5d) shifted from 1027 cm^{-1} in the UG sample to 1008 cm^{-1} in the RG10 sample and 1010 cm^{-1} in the BRG sample. The shift to lower frequencies was expected based on previous studies of dithionite-reduced smectites (Stucki and Roth, 1976; Russell *et al.*, 1979; Komadel *et al.*, 1990; Yan and Stucki, 2000; Fialips *et al.*, 2002b). Reoxidation returned the Si–O-stretching band of ROG10 and BROG to virtually the same position as before reduction (Figure 5d).

Ferruginous smectite

OH-stretching vibration bands. The OH-stretching band in unaltered SWa-1 (US), centered at 3576 cm^{-1} (Figure 3), was much broader than in unaltered Garfield due to the greater octahedral Al and Mg contents in SWa-1, giving more [AlAl]OH and [AlMg]OH configurations which vibrate at higher frequencies (~3652–3618 cm^{-1}) than the Fe analogs (Goodman *et al.*, 1976; Madejová *et al.*, 1994; Fialips *et al.*, 2002a). Madejová *et al.* (1994) and Fialips *et al.* (2002b) successfully deconvoluted the main envelope of US into at least five components. They observed that the most intense component band was the $[Fe(III)]_2$OH-stretching vibration at ~3565–3532 cm^{-1}, followed by [AlFe(III)]OH as the next most intense band at ~3611–3587 cm^{-1}. These two components accounted for ~75% of the total integrated area of the peak.

Reduction of SWa-1 by dithionite for 10 min (RS10) or by bacteria (BRS) produced reduction levels of 0.985 and 0.886 mmol Fe(II)/g clay (Table 5), respectively, and the overall band for the structural OH-stretching vibrations was broadened slightly towards the low-

Table 3. Positions (cm^{-1}) and relative spectral areas (A) of the OH-stretching bands of the unaltered (US), bacteria-reduced (BRS), and 10 min dithionite-reduced (RS10) ferruginous smectite (Swa-1).

Band	Assignment	US		BRS		RS10	
		(cm^{-1})	A (%)	(cm^{-1})	A (%)	(cm^{-1})	A (%)
1	AlMgOH	3703	0.3	3702	0.8	3703	0.3
2	AlAlOH	3652	12.6	3655	10.5	3647	12.9
3	AlMgOH	3627	4.8	3627	4.7	3626	6.1
4	FeAlOH	3603	28.1	3601	28.3	3699	23.0
5	FeMgOH	3581	5.4	3580	8.1	3581	4.4
6	FeFeOH	3559	48.8	3562	39.1	3562	20.2
7	FeFeOH	–	–	3541	8.5	3537	33.1
Total			100.0		100.0		100.0

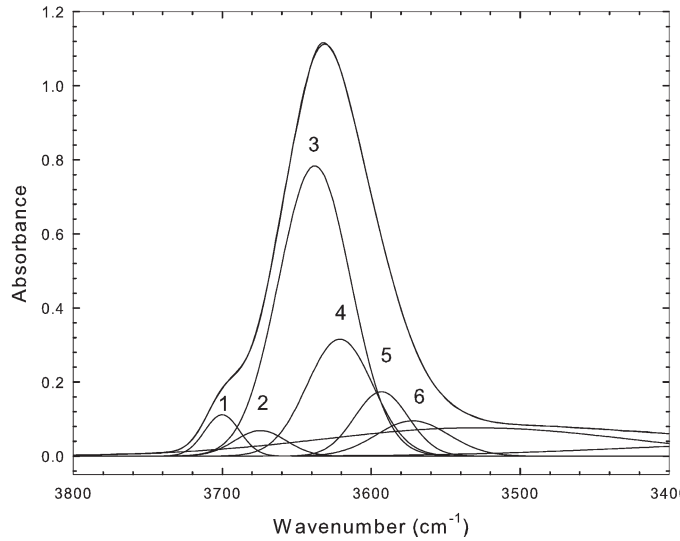

Figure 4. IR spectrum of the OH-stretching region in unaltered Upton montmorillonite (UU) deconvoluted to reveal the peak positions for the possible M_2OH environments. Band assignments and areas are reported in Table 4.

frequency side and its intensity decreased (Figure 6a) after either treatment (BRS or RS10). The overall position of the band was largely unchanged in the bacteria-reduced sample (BRS), but dithionite reduction for 10 min (sample RS10) shifted the peak slightly towards lower frequency. Both treatments yielded peaks in which the split between contributions from Fe(III)Fe(III), Fe(II)Fe(III) and Fe(II)Fe(II) was evident by the accentuation of multiple components under the overall peak. The sharper differentiation between the components in RS10 compared to BRS is probably the result of a difference in Fe(II) distribution within the octahedral sheet, as the same Fe(II) content could be achieved with Fe(II) being distributed more within Fe(II)Fe(II) pairs than within Fe(II)Fe(III) pairs, or *vice versa*. The rising background on the low-frequency side of the peak in BRS evidently derives from residual bacterial cells and/or culture medium because it is also present in the bacteria-reduced Garfield sample (Figure 6a), but is absent from samples untreated by bacteria. The specific origin for this background, however, was not determined.

Reoxidation of samples BRS and RS10 failed to restore the OH-stretching band (Figure 6b) to its original position and shape found in sample US, but the effects of bacterial and dithionite reduction were similar in this regard. The peak after reoxidation had a more prominent intensity on the high-frequency side compared to the unaltered sample. Some redistribution of the metal cation environments of the OH groups may have occurred, *i.e.* more [AlAl]OH and, perhaps, [AlMg]OH configurations were evident in reoxidized samples BROS and ROS10 than in the unaltered sample US. Cationic configurations were, therefore, perturbed on initial reduction and were at least partially irreversible upon reoxidation.

OH-bending vibration bands. The two most prominent bands in the $[M]_2$–O–H deformation region of SWa-1 (Figure 6c), at 875 cm^{-1} and 822 cm^{-1}, are assigned to

Table 4. Positions (cm^{-1}) and relative spectral areas (A) of the OH-stretching bands of the unaltered (UU), bacteria-reduced (BRU), and 120 min dithionite-reduced (RU120) Upton montmorillonite.

Band	Assignment	UU		BRU		RU120	
		(cm^{-1})	A (%)	(cm^{-1})	A (%)	(cm^{-1})	A (%)
1	AlMgOH	3700	4.0	–	–	–	–
2*	M_3 + H_2O	3674	–	3672	–	3674	–
3	AlAlOH	3638	58.0	3630	59.7	3629	54.8
4	AlMgOH	3621	21.4	3615	21.1	3608	22.7
5	AlFeOH	3593	9.6	3589	12.1	3580	9.2
6	FeMgOH or FeFeOH	3572	7.0	3568	7.1	3564	4.8
Total			100.0		100.0		91.5

* The area of band No. 2 was excluded from the total area of the OH-stretching bands.

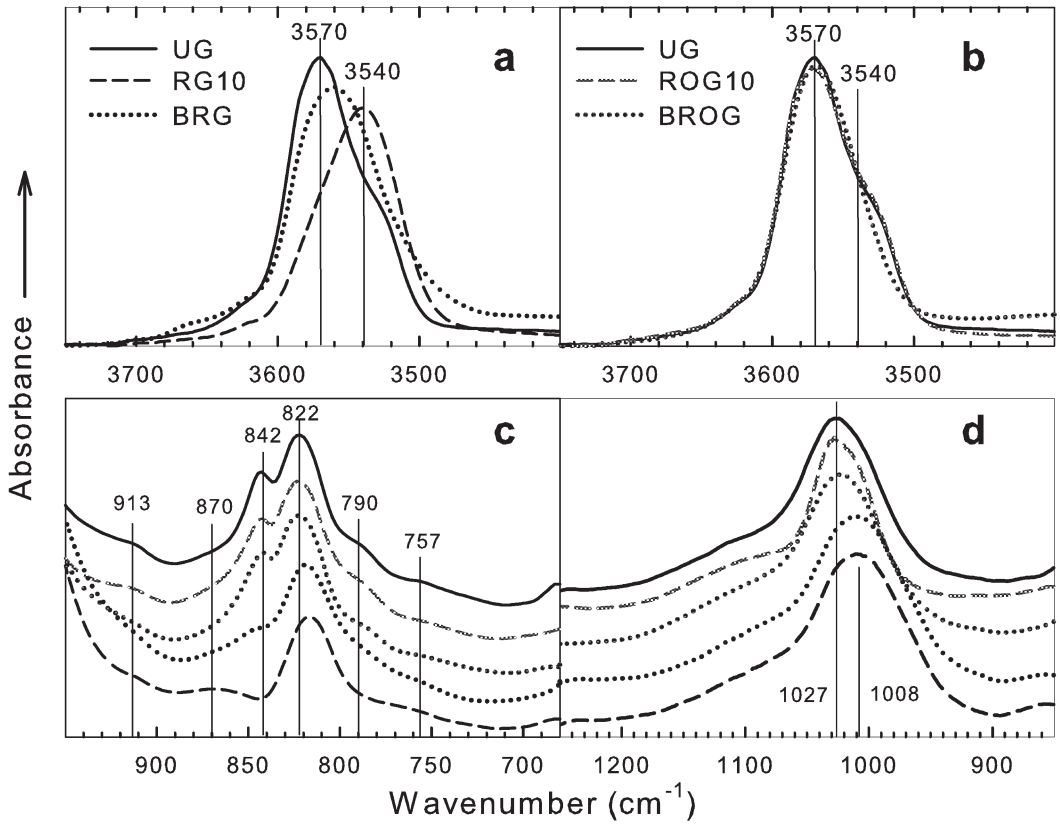

Figure 5. IR spectra of vibrational bands in Garfield nontronite. (a) Normalized OH-stretching bands of unaltered (UG), reduced by bacteria (BRG), and reduced by dithionite for 10 min (RG10). (b) Normalized OH-stretching bands of unaltered (UG); reduced by bacteria, then reoxidized (BROG); and reduced by dithionite for 10 min, then reoxidized (ROG10). (c) Normalized M_2–O–H deformation bands of unaltered (UG); reduced by bacteria (BRG); reduced by dithionite for 10 min (RG10); reduced by bacteria, then reoxidized (BROG); and reduced by dithionite for 10 min, then reoxidized (ROG10). (d) Si–O stretching bands of unaltered (UG); reduced by bacteria (BRG); reduced by dithionite for 10 min (RG10); reduced by bacteria, then reoxidized (BROG); and reduced by dithionite for 10 min, then reoxidized (ROG10).

[AlFe(III)]–O–H and $[Fe(III)]_2$–O–H groups, respectively (Serratosa, 1960; Goodman *et al.*, 1976; Russell *et al.*, 1979; Fialips *et al.*, 2002a). The apparent intensity ratio of these two bands is, however, contrary to the ratio of Fe(III) to Al determined by chemical analysis. Madejová *et al.* (1994) estimated that the FeAl octahedral pairs accounted for only 14.5% of the area of the OH-stretching band in SWa-1. Fialips *et al.* (2002b) postulated that the apparent discrepancies in relative intensities of the 875 and 822 cm^{-1} bands could be due to differences in their absorption coefficients. The weak band at 921 cm^{-1} is assigned to $[Al]_2$–O–H (Farmer and Russell, 1964; Goodman *et al.*, 1976) and bands at 844 and 791 cm^{-1} are probably of the same, even though uncertain, origin as in Garfield (see above).

No discernible differences were found between the effects of bacterial and dithionite reduction on the $[M]_2$–O–H deformation modes (Figure 6c). While the position of the peak at 875 cm^{-1} was unaffected by structural Fe reduction, its relative intensity decreased measurably upon reduction and was restored by reoxidation (Figure 6c). The peak at 844 cm^{-1} was lost upon reduction by both agents and only partially reappeared upon reoxidation. The bands at 822 cm^{-1} and 921 cm^{-1} shifted slightly to lower frequencies in the reduced samples (BRS and RS10) and returned to their normal state after reoxidation (samples BROS and ROS10).

Si–O-stretching vibration bands. The position of the Si–O-stretching band of US (Figure 6d) was at a slightly greater frequency (1035 cm^{-1}) than in UG (1027 cm^{-1}). The favored attribution for this shift relative to UG is to differences in the octahedral cations that are coordinated to the apical oxygens. Goodman *et al.* (1976) suggested that an upwards shift in Si–O-stretching frequencies may be due to a decrease in tetrahedral Fe, but this explanation appears unlikely in this case because the preponderance of evidence indicates that Garfield contains virtually no tetrahedral Fe(III) and, even though the presence of tetrahedral Fe(III) in SWa-1 has yet to be completely ruled out, it is highly unlikely to be less than in Garfield (Manceau *et al.*, 2000).

The position of the Si–O-stretching band shifted to lower frequency with Fe reduction, from 1035 cm^{-1} in

Table 5. Measured reduction levels of unaltered, reduced, and reduced-reoxidized smectites.

	Structural Fe(II) in smectite					
	Garfield		SWa-1		Upton	
Reduction treatment	Fe(II)/ total Fe	mmol Fe(II)/ g clay	Fe(II)/ total Fe	mmol Fe(II)/ g clay	Fe(II)/ total Fe	mmol Fe(II)/ g clay
Unaltered (no treatment)	0.0027	0.012	0.0037	0.012	0.0625	0.027
Bacteria reduced	0.17	0.735	0.27	0.886	0.87	0.374
Bacteria reduced, reoxidized	0.02	0.087	0.01	0.033	0.04	0.017
Dithionite reduced (10 min)	0.23	0.995	0.30	0.985	0.38	0.163
Dithionite reduced (10 min), reoxidized	0.01	0.043	0.01	0.033	0.02	0.009
Dithionite reduced (120 min)	n.d.	n.d.	n.d.	n.d.	0.91	0.391
Dithionite reduced (120 min), reoxidized	n.d.	n.d.	n.d.	n.d.	0.02	0.009
Dithionite reduced (240 min)	n.d.	n.d.	n.d.	n.d.	0.95	0.408
Dithionite reduced (240 min), reoxidized	n.d.	n.d.	n.d.	n.d.	0.02	0.009

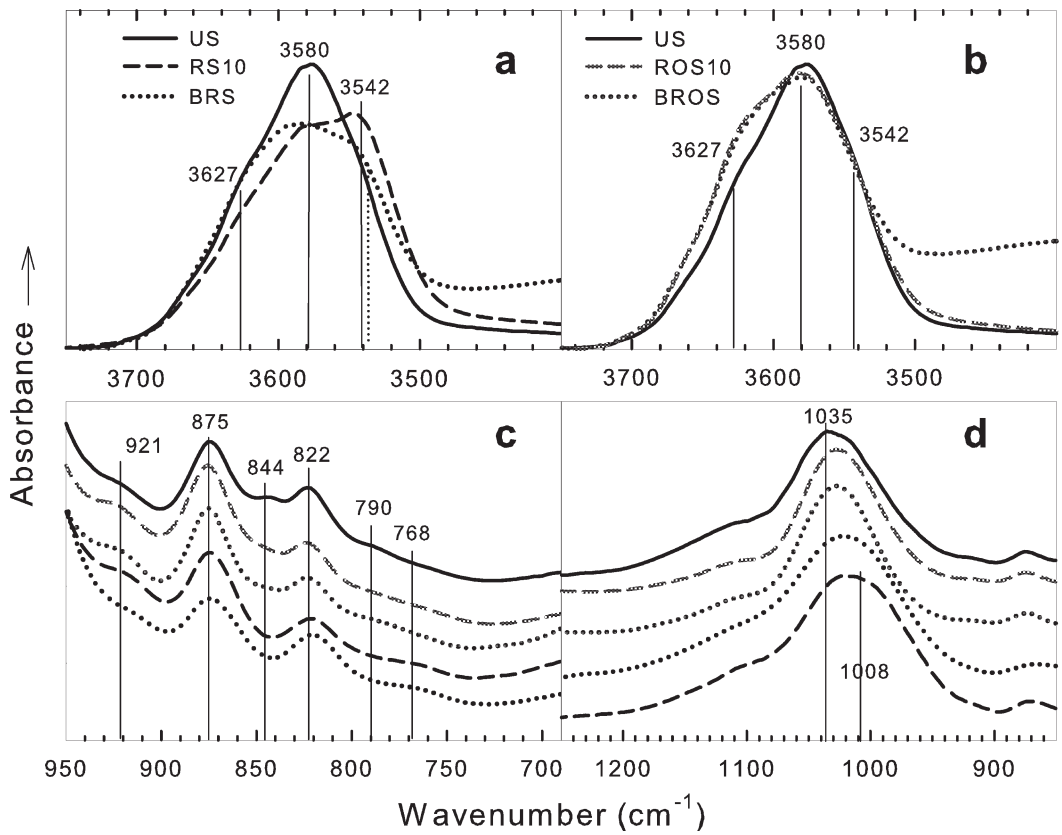

Figure 6. IR spectra of vibrational bands in ferruginous smectite (SWa-1). (a) Normalized OH-stretching bands of unaltered (US), reduced by bacteria (BRS), and reduced by dithionite for 10 min (RS10). (b) Normalized OH-stretching bands of unaltered (US); reduced by bacteria, then reoxidized (BROS); and reduced by dithionite for 10 min, then reoxidized (ROS10). (c) Normalized M_2−O−H deformation bands of unaltered (US); reduced by bacteria (BRS); reduced by dithionite for 10 min (RS10); reduced by bacteria, then reoxidized (BROS); and reduced by dithionite for 10 min, then reoxidized (ROS10). (d) Si−O-stretching bands of unaltered (US); reduced by bacteria (BRS); reduced by dithionite for 10 min (RS10); reduced by bacteria, then reoxidized (BROS); and reduced by dithionite for 10 min, then reoxidized (ROS10).

US to 1020 cm^{-1} in the RS10 and 1024 cm^{-1} in BRS (Figure 6d). Upon reoxidation (Figure 6d), the Si–O band in ROS10 and BROS shifted back to higher frequencies, but failed to recover completely to the original position observed in US. No analysis of the relative intensities was possible due to the overlap of bacterial polysaccharide peaks (Figure 1).

Upton montmorillonite

The level of reduction achieved in Upton montmorillonite by dithionite typically requires a longer treatment to achieve the same levels of reduction than in Garfield or SWa-1. In the current study, Upton was submitted to dithionite treatments for 10, 120 and 240 min, and produced reduction levels of 0.163, 0.391 and 0.408 mmol Fe(II)/g clay, respectively (Table 5). Bacterial reduction yielded a maximum of 0.374 mmol Fe(II)/g. Reduction treatments created noticeable changes in the IR spectra of Upton, as described below but the spectra from the three dithionite treatments were largely indistinguishable from one another (Figure 7a). As the 120 min treatment produced a comparable reduction level to bacterial treatment, this appears to be the appropriate sample with which to make comparison with bacteria reduction. The total amount of Fe(II) produced by bacterial reduction in Upton was less than in either Garfield (0.735 mmole Fe(II)/g clay) or SWa-1 (0.886 mmole Fe(II)/g clay); but, interestingly, only a 10 min dithionite treatment was required to reduce either Garfield or SWa-1 to the corresponding levels achieved with bacteria (Table 5).

OH-stretching vibration bands. The OH-stretching band in unaltered Upton montmorillonite sample UU (Figure 4) was centered at 3632 cm^{-1}, and is at a higher frequency than in UG and US because of its greater octahedral Al and Mg and lesser octahedral Fe contents. The possible coordination environments for OH are [AlAl]OH, [AlMg]OH, [AlFe]OH, [MgFe]OH and possibly [MgMg]OH. The lack of color change of this sample upon Fe reduction is further evidence that [FeFe]OH environments are absent (Komadel *et al.*, 1990).

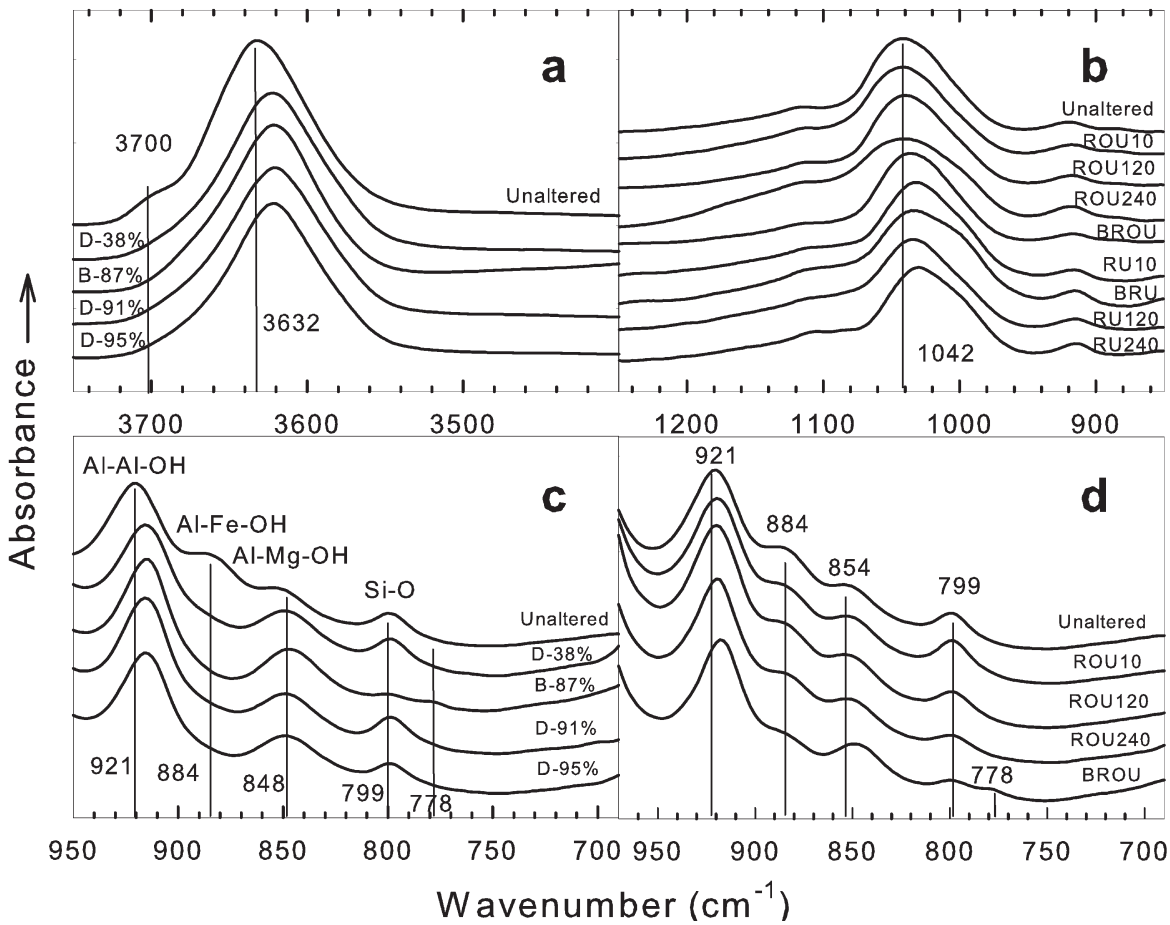

Figure 7. IR vibrational bands in Upton montmorillonite. (a) Normalized OH-stretching bands of dithionite reduced to various levels (RU) and bacteria reduced (BRU). (b) Si–O-stretching bands of dithionite and bacteria reduced and reoxidized. (c) M_2–O–H-bending bands of dithionite reduced to various levels (RU) and bacteria reduced (BRU). (d) M_2–O–H-bending bands of dithionite-reduced to various levels, then reoxidized (ROU) and bacteria-reduced, then reoxidized (BROU).

The unaltered sample invariably contains a measurable amount of Fe(II) (Table 5), which could cause the overall position of the OH-stretching band of the unaltered sample to be at a slightly lower frequency than if all of the Fe were Fe(III). Structural Fe reduction by bacteria or dithionite shifted the OH-stretching band downwards by ~12 cm^{-1} to 3620 cm^{-1} (Figure 7a) and decreased its intensity by ~8.5% (Table 4). If no change in absorptivity of the OH-stretching band occurred, this would indicate a small amount of structural dehydroxylation during reduction.

The overall shift in peak position with reduction is attributed generally to the conversion of Fe(III)*M*OH to Fe(II)*M*OH environments (where *M* is Al or Mg), but changes are also observed in the bands associated with octahedral Al and/or Mg. For example, the shoulder at 3700 cm^{-1} in the UU sample disappeared upon reduction (Figure 7a), but was restored after reoxidation (Figure 8). This sensitivity of the high-energy side of the OH-stretching peak to Fe reduction is surprising in the sense that bands in this region typically derive from either trioctahedral configurations, which are unexpected in dioctahedral Upton, or are not directly related to Fe. This result is consistent with nuclear magnetic resonance (NMR) results of Gates *et al.* (1996), who found perturbations in the magic-angle spinning NMR spectrum of octahedral Al of Upton montmorillonite when reduced by either dithionite or *pseudomonas* bacteria. They explained the perturbation on Al as being due to either a lessening of the paramagnetic influence of Fe on Al (reducing Fe(III) to Fe(II) decreases the number of unpaired electrons on the Fe) or to the enhancement of signals from Al with different quadrupole coupling constants. Either of these phenomena would perturb the energies and/or symmetries of all bonds in the sheet, including next-nearest and next-next-nearest neighbors to the Fe, regardless of the cation occupying the site. Such perturbations would alter the vibrational energies and account for the observed shifts (Figure 7a). A similar effect was also manifested in the M_2–O–H deformation region as described below. Reoxidation restored the spectrum of the Upton montmorillonite completely to its original state (Figure 8).

OH-bending vibration bands. The most pronounced deformation band in the unaltered Upton, at 921 cm^{-1}, was assigned to an octahedral $[Al]_2$–O–H environment, in accordance with the high octahedral Al content (Figure 7c). Other bands were found at 884, 854 and 799 cm^{-1} and assigned to [AlFe(III)]–O–H,

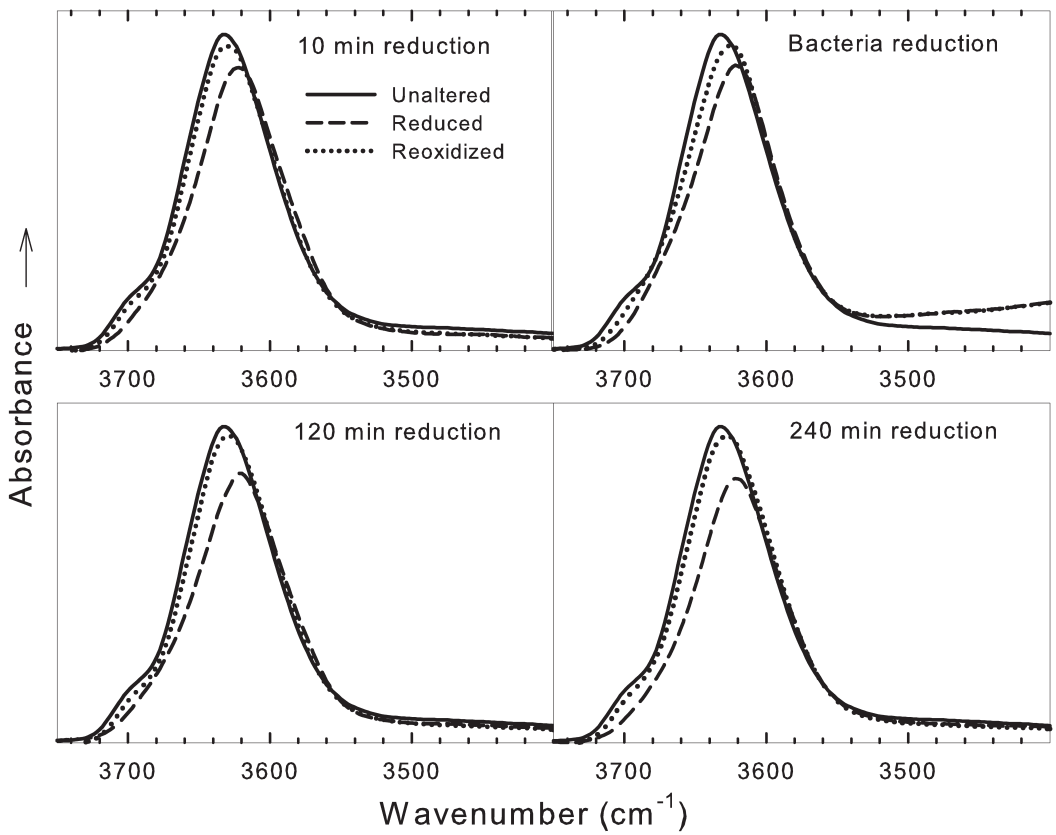

Figure 8. Normalized IR spectra of OH-stretching bands in dithionite reduced-reoxidized and bacteria reduced-reoxidized Upton montmorillonite.

[AlMg]−O−H, and [Si−O] associated with finely divided quartz, respectively (Stubican and Roy, 1961; Farmer and Russell, 1964; Russell *et al.*, 1970; Farmer, 1974). The relatively lower intensity of the [AlFe(III)]−O−H band at 884 cm^{-1} compared to the [AlAl]−O−H band indicates fewer Al-Fe pairs compared to Al-Al pairs in the structure. The 884 cm^{-1} band disappeared from the spectrum for Upton at all levels of reduction that were investigated (Figure 7c), whereas it persisted in Garfield (Figure 5c) and SWa-1 (Figure 6c). Reduction by bacteria or dithionite produced a downward shift of the 921 cm^{-1} band to 916 cm^{-1} and removed the 884 cm^{-1} band. A new, small band appeared in the bacteria-reduced sample at 778 cm^{-1}. Reoxidation restored all of the peaks to approximately their original positions, except the 778 cm^{-1} peak persisted in the bacteria-reduced-reoxidized sample (Figure 7d).

While a shift in peak positions in the $[M]_2$−O−H deformation region with Fe reduction is expected, as observed in Garfield and SWa-1 (even with a relatively small extent of reduction), the observed shift in the $[Al]_2$−O−H band is surprising because that band is unrelated to Fe. This sensitivity of Al sites to changes occurring in the Fe sites is, however, consistent with the change in the 3700 cm^{-1} band observed in the OH-stretching region, as described above, and provides more evidence that reduction of Fe must perturb non-Fe octahedral sites. Shifts in the Si−O vibrational modes (see below) are further testimony that perturbations extend beyond the Fe sites.

Si−O-stretching vibration bands. The Si−O-stretching band in unaltered Upton is positioned at 1042 cm^{-1} (Figure 7b), which is a higher frequency than observed in the more Fe-rich smectites (Figures 5d, 6d). Both dithionite (120 min) and bacterial reduction shifted this band downwards by 12 cm^{-1} to 1030 cm^{-1}, which is less than observed in Garfield (43 cm^{-1}) and SWa-1 (45 cm^{-1}), and indicates that the effect of Fe reduction on the overall smectite is greater in the Fe-rich smectite and nontronite than in the lower Fe montmorillonite. Stucki and Roth (1976), Gates *et al.* (1996), Yan and Stucki (1999, 2000) and Fialips *et al.* (2002a, 2000b) observed a similar phenomenon. It further indicates that bacterial reduction invokes only minor changes in smectite structure and the changes are comparable to those observed at similar levels of reduction by dithionite.

CONCLUSIONS

The effects of bacteria-mediated Fe reduction on the structure of three Fe-bearing smectites (Garfield nontronite, ferruginous smectite SWa-1 and Upton montmorillonite) were investigated using FTIR spectroscopy and compared with results obtained from similar levels of reduction using dithionite as the reducing agent. The levels of bacterial reduction achieved were 0.735, 0.886 and 0.374 mmole Fe(II)/g clay for Garfield, SWa-1 and Upton, respectively. The general behavior observed in all three spectral regions investigated, *i.e.* OH-stretching, M_2−O−H deformation, and Si−O stretching, for bacteria-reduced smectite was that the effects on smectite structure were minor and similar to those observed at comparable levels of reduction by dithionite. In particular, (1) the OH-stretching band generally shifted to lower frequency in the reduced clays and lost intensity, possibly due to partial dehydroxylation; (2) M_2−O−H deformation bands linked to Fe shifted and lost intensity upon reduction, except for Upton in which changes were minimal; (3) the Si−O-stretching band shifted to lower frequency; and (4) reoxidation largely restored the bands in all three regions to their unaltered positions and intensities. Results from Upton montmorillonite revealed that Fe reduction also perturbs the vibrational spectra of crystal structure sites occupied by Al, Mg and Si ions.

In summary, bacterial reduction of Fe-bearing smectites changes the clay structure, but the changes are largely reversed upon reoxidation. Redox cycles mediated by the bacteria are, therefore, likely to produce few, if any, lasting changes in the structure and composition of Fe-bearing smectites. This generalization is valid for levels of reduction up to ~1 mmole Fe/g clay, but further study is required to determine the structural changes that occur if the level of reduction exceeds this value or if organic ligands/chelates are present. Comparisons of biotic and abiotic reduction under similar buffer conditions and a similar time frame are warranted.

ACKNOWLEDGMENTS

This study was supported by The International Arid Lands Consortium, Grant No. 03R-15; BARD; The United States-Israel Binational Agricultural Research and Development Fund, Research Grant Award No. AG IS-3162-99R; the National Science Foundation, Division of Petrology and Geochemistry, Grant No. EAR 01-26308; and the Natural and Accelerated Bioremediation Research (NABIR) Program, Biological and Environmental Research (BER), US Department of Energy, Grant No. DE-FG02-00ER62986, subcontract FSU F48792.

REFERENCES

Angell, C.L. and Schaffer, P.C. (1965) Infrared spectroscopic investigations of zeolites and adsorbed molecules. I. Structural OH groups. *Journal of Physical Chemistry*, **69**, 3463−3470.

Benning, L.G., Phoenix, V.R., Yee, N. and Tobin, M.J. (2004) Molecular characterization of cyanobacterial silicification using synchrotron infrared micro-spectroscopy. *Geochimica et Cosmochimica Acta*, **68**, 729−741.

Boivin, P., Favre, F., Hammecker, C., Maeght, J.L., Delariviere, J., Poussin, J.C. and Wopereis, M.C.S. (2002) Processes driving soil solution chemistry in a flooded rice-cropped vertisol: analysis of long-time monitoring data.

Geoderma, **110**, 87–107.

Choo-Smith, L.-P., Maquelin, K., Van Vreeswijk, T., Brunning, H.A., Puppels, G.J., Ngo Thi, N.A., Kirschner, C., Naumann, D., Ami, D., Villa, A.M., Orsini, F., Doglia, S.M., Lamfarraj, H. and Sockalingum, G.D. (2001) Investigating microbial (mciro)colony heterogeneity by vibrational spectroscopy. *Applied and Environmental Microbiology*, **67**, 1461–1469.

Dong, H., Kostka, J.E. and Kim, J. (2003) Microscopic evidence for microbial dissolution of smectite. *Clays and Clay Minerals*, **51**, 502–512.

Farmer, V.C. (1974) *Infrared Spectra of Minerals*. Monograph **4**, The Mineralogical Society, London, 524 pp.

Farmer, V.C. and Russell, J.D. (1964) The infra-red spectra of layer silicates. *Spectrochimica Acta*, **20**, 1149–1173.

Favre, F., Tessier, D., Abdelmoula, M., Genin, J.M., Gates, W.P. and Boivin, P. (2002) Iron reduction and changes in cation exchange capacity in intermittently waterlogged soil. *European Journal of Soil Science*, **53**, 175–183.

Favre, F., Jaunet, A.M., Pernes, M., Badraoui, M., Boivin, P. and Tessier, D. (2004) Changes in clay organization due to structural iron reduction in a flooded vertisol. *Clay Minerals*, **39**, 123–134.

Fialips, C.-I., Huo, D., Yan, L., Wu, J. and Stucki, J.W. (2002a) Infared study of reduced and reduced-reoxidized ferruginous smectite. *Clays and Clay Minerals*, **50**, 455–469.

Fialips, C.-I., Huo, D., Yan, L., Wu, J. and Stucki, J.W. (2002b) Effect of iron oxidation state on the IR spectra of Garfield nontronite. *American Mineralogist*, **87**, 630–641.

Gates, W.P. (2005) Infrared spectroscopy and the chemistry of dioctahedral smectites. Pp. 125–168 in: *The Application of Vibrational Spectroscopy to Clay Minerals and Layered Double Hydroxides* (J.T. Kloprogge, editor). CMS Workshop Lectures, Vol. **13**. The Clay Minerals Society, Aurora, CO.

Gates, W.P., Stucki, J.W. and Kirkpatrick, R.J. (1996) Structural properties of reduced Upton montmorillonite. *Physics and Chemistry of Minerals,* **23**, 535–541.

Goodman, B.A., Russell, J.D., Fraser, A.R. and Woodhams, F.D. (1976) A Mössbauer and I.R. spectroscopic study of the structure of nontronite. *Clays and Clay Minerals*, **24**, 53–59.

Huo, D. (1997) Infrared study of oxidized and reduced nontronite and Ca-K competition in the interlayer. PhD Dissertation, University of Illinois, Urbana.

Huo, D., Fialips, C.-I. and Stucki, J.W. (2004) Effects of structural Fe oxidation state on physical-chemical properties of smectites: evidence from infrared spectroscopy. *Japanese Society of Soil Physics*, **96**, 3–10.

Kim, J., Furukawa, Y., Daulton, T.E., Lavoie, D. and Newell, S.W. (2003) Characterization of microbially Fe(III) reduced nontronite: environmental cell-transmission electron microscopy study. *Clays and Clay Minerals*, **51**, 382–389.

Kim, J., Dong, H., Seabaugh, J., Newell, S.W. and Eberl, D.D. (2004) Role of microbes in the smectite to illite reaction. *Science*, **303**, 830–832.

Kirschner, C., Maquelin, K., Pina, P., Ngo Thi, N.A., Choo-Smith, L.-P., Sockalingum, G.D., Sandt, C., Ami, D., Orsini, F., Doglia, S.M., Allouch, P., Mainfait, M., Puppels, G.J. and Naumann, D. (2001) Classification and identification of enterococci: a comparative phenotypic, genotypic and vibrational spectroscopic study. *Journal of Clinical Microbiology,* **39**, 1763–1770.

Komadel, P. and Stucki, J.W. (1988) Quantitative assay of minerals for Fe^{2+} and Fe^{3+} using 1,10-phenanthroline: III. A rapid photochemical method. *Clays and Clay Minerals,* **36**, 379–381.

Komadel, P., Lear, P.R. and Stucki, J.W. (1990) Reduction and reoxidation of nontronite: Extent of reduction and reaction rates. *Clays and Clay Minerals*, **38**, 203–208.

Kostka, J.E. (2002) Growth of iron(III)-reducing bacteria on clay minerals as the sole electron acceptor and comparison of growth yields on a variety of oxidized iron forms. *Applied and Environmental Microbiology*, **68**, 6256–6262.

Kostka, J. and Nealson, K.H. (1998) Isolation, cultivation and characterizations of iron- and manganese-reducing bacteria. Pp. 58–78 in: *Techniques in Microbial Ecology* (R.S. Burlage, R. Atlas, D. Stahl, G. Geesey and G. Sayler, editors). Oxford University Press, New York.

Kostka, J.E., Stucki, J.W., Nealson, K.H. and Wu, J. (1996) Reduction of structural Fe(III) in smectite by a pure culture of the Fe-reducing bacterium Shewanella putrefaciens strain MR-1. *Clays and Clay Minerals*, **44**, 522–529.

Kostka, J.E., Haefele, E., Viehweger, R. and Stucki, J.W. (1999) Respiration and dissolution of Fe(III)-containing clay minerals by bacteria. *Environmental Science and Technology*, **33**, 3127–3133.

Madejová, J., Komadel, P. and Čičel, B. (1994) Infrared study of octahedral site populations in smectites. *Clay Minerals*, **29**, 319–326.

Manceau, A., Lanson, B., Drits, V.A., Chateigner, D., Gates, W.P., Wu, J., Huo, D. and Stucki, J.W. (2000a) Oxidation-reduction mechanism of iron in dioctahedral smectites. 1. Crystal chemistry of oxidized reference nontronites. *American Mineralogist*, **85**, 133–152.

Manceau, A., Lanson, B., Drits, V.A., Chateigner, D., Wu, J., Huo, D., Gates, W.P. and Stucki, J.W. (2000b) Oxidation-reduction mechanism of iron in dioctahedral smectites. 2. Structural chemistry of reduced Garfield nontronite. *American Mineralogist*, **85**, 153–172.

Maquelin, L., Kirschner, C., Choo-Smith, L.-P., van den Braak, N., Endtz, H.Ph., Naumann, D. and Puppels, G.J. (2002) Identification of medically relevant microorganisms by vibrational spectroscopy. *Journal of Microbiological Methods*, **51**, 255–271.

Myers, C.R. and Nealson, K.H. (1988) Bacterial manganese reduction and growth with manganese oxide as the sole electron acceptor. *Science*, **240**, 1319–1321.

Nealson, K.H. and Saffarini, D. (1994) Iron and magnanese in anaerobic respiration: Environmental significance, physiology and regulation. *Annual Reviews in Microbiology*, **48**, 311–343.

Robert, J.-J. and Kodama, H. (1988) Generalization of the correlations between hydroxyl-stretching wavenumbers and composition of micas in the system K_2O-MgO-Al_2O_3-SiO_2-H_2O: a single model for trioctahedral and dioctahedral micas. *American Journal of Science*, **288A**, 196–212.

Russell, J.D., Farmer, V.C. and Velde, B. (1970) Replacement of OH by OD in layer silicates, and identification of the vibrations of these groups in infrared spectra. *Mineralogical Magazine*, **37**, 869–879.

Russell, J.D., Goodman, B.A. and Fraser, A.R. (1979) Infrared and Mössbauer studies of reduced nontronites. *Clays and Clay Minerals*, **27**, 63–71.

Scott, J.H. and Nealson, K.H. (1994) A biochemical study of the intermediary carbon metabolism of Shewanella putrefaciens. *Journal of Bacteriology*, **176**, 3408–3411.

Serratosa, J.M. (1960) Dehydration studies by infrared spectrosopy. *American Mineralogist*, **45**, 1101–1104.

Stubican, V. and Roy, R. (1961) Isomorphous substitution and infrared spectra of the layer silicates. *American Mineralogist*, **46**, 32–51.

Stucki, J.W. and Getty, P.J. (1986) Microbial reduction of iron in nontronite. *Agronomy Abstracts*, **1986**, 279.

Stucki, J.W. and Roth, C.B. (1976) Interpretation of infrared spectra of oxidized and reduced nontronite. *Clays and Clay Minerals*, **24**, 293–296.

Stucki, J.W. and Roth, C.B. (1977) Oxidation-reduction mechanism for structural iron in nontronite. *Soil Science Society of America Journal*, **41**, 808–814.

Stucki, J.W., Komadel, P. and Wilkinson, H.T. (1987) Microbial reduction of structural iron(III) in smectites. *Soil Science Society of America Journal*, **51**, 1663–1665.

Vantelon, D., Pelletier, M., Michot, L.J., Barres, O. and Thomas, F. (2001) Fe, Mg, and Al distribution in the octahedral sheet of montmorillonites. An infared study in the OH-bending region. *Clay Minerals*, **36**, 369–379.

Wu, J., Roth, C.B. and Low, P.F. (1988) Biological reduction of structural Fe in sodium-nontronite. *Soil Science Society of America Journal*, **52**, 295–296.

Yan, L. and Stucki, J.W. (1999) Effects of structural Fe oxidation state on the coupling of interlayer water and structural Si-O stretching vibrations in montmorillonite. *Langmuir*, **15**, 4648–4657.

Yan, L. and Stucki, J.W. (2000) Structural perturbations in the solid-water interface of redox transformed nontronite. *Journal of Colloid and Interface Science*, **225**, 429–439.

Yan, L., Low, P.F. and Roth, C.B. (1996a) Enthalpy changes accompanying the collapse of montmorillonite layers and the penetration of electrolyte into interlayer space. *Journal of Colloid and Interface Science*, **182**, 417–424.

Yan, L., Low, P.F. and Roth, C.B. (1996b) Swelling pressure of montmorillonite layers versus H-O-H bending frequency of the interlayer water. *Clays and Clay Minerals*, **44**, 749–765.

Yan, L., Roth, C.B. and Low, P.F. (1996c) Changes in the Si-O vibrations of smectite layers accompanying the sorption of interlayer water. *Langmuir*, **12**, 4421–4429.

Yan, L., Roth, C.B. and Low, P.F. (1996d) Effects of monovalent, exchangeable cations and electrolytes on the infrared vibrations of smectite layers and interlayer water. *Journal of Colloid and Interface Science*, **184**, 663–670.

(*Received 15 April 2005; revised 15 November 2005; Ms. 1040; A.E. W. P. Gates*)